



1 **Impacts of Simulated Coastal Ocean Alkalinity Enhancement on the Seasonal Cycle of the**  
2 **Air-Sea CO<sub>2</sub> Flux and Surface Ocean pCO<sub>2</sub> in European Waters under a Low- and a**  
3 **High-Emission Scenario**

4

5 Chiara Ciscato 1,2, Neha Mehendale 2,4, Tronje P. Kemena 2, Sandy Avrutin 2, David P. Keller 2,3

6

7 1 CMCC Foundation - Euro-Mediterranean Center on Climate Change (Italy)

8 2 GEOMAR Helmholtz Centre for Ocean Research, Kiel (Germany)

9 3 Carbon to Sea Initiative, Washington, DC (USA)

10 4 Institute for Environmental Physics, University of Bremen (Germany)

11

12

13

14 Key Points:

15

16 • Ocean Alkalinity Enhancement (OAE) aims to increase the ocean's potential to  
17 sequester and store atmospheric CO<sub>2</sub>

18 • In our study area, OAE effects are strongest in enhancing CO<sub>2</sub> uptake in winter and in  
19 lowering ocean pCO<sub>2</sub> in summer

20 • The sensitivity of the seasonal carbon cycle increases under higher CO<sub>2</sub> emissions

21

22

23

24

25

26 Corresponding author: Chiara Ciscato, [chiara.ciscato@cmcc.it](mailto:chiara.ciscato@cmcc.it)



27 Abstract

28 One potentially scalable method to remove CO<sub>2</sub> from the air is ocean alkalinity  
29 enhancement (OAE), which works to lower surface ocean partial pressure (pCO<sub>2</sub>) and  
30 accelerate CO<sub>2</sub> sequestration and durable storage. This study explores how OAE might  
31 affect the seasonal carbon cycle, which plays a key role in the ocean's annual CO<sub>2</sub> uptake.  
32 By analysing earth system model simulations of OAE implemented continuously at the  
33 European coastline until 2100 under low and high climate forcing, it was found that: when  
34 carbon cycle seasonality is temperature-driven, a) OAE enhances CO<sub>2</sub> uptake in winter,  
35 when it is naturally strongest, and it reduces ocean pCO<sub>2</sub> in summer, when it is naturally  
36 highest; b) higher CO<sub>2</sub> emissions increase the sensitivity of the seasonal carbon cycle; c) a  
37 region with a shallow bathymetry and well-mixed waters may be ideal for implementing  
38 OAE due to fast air-sea CO<sub>2</sub> equilibration.

39

40 Short summary

41 While reducing emissions, technologies are being developed to sequester carbon  
42 dioxide (CO<sub>2</sub>) from the air. Among the proposed options is ocean alkalinity enhancement  
43 (OAE), which works to lower the CO<sub>2</sub> concentration in seawater and accelerate its uptake  
44 from the atmosphere as a compensatory effect. As seasonality is important for the annual  
45 air-sea CO<sub>2</sub> exchange, this research investigates OAE impacts on the seasonal carbon  
46 cycle analysing outputs from a numerical earth system model.

47

48

49

50

51

52

53

54

55

56

57

58

59



60 1 Introduction

61 The ocean constitutes a valuable resource for climate stabilisation, absorbing much of  
62 the earth's excess heat and storing vast amounts of carbon in its interior and deep waters  
63 (Friedlingstein et al., 2022; Scott-Buechler & Greene, 2019). Thus, research on marine  
64 carbon dioxide removal (CDR) has been expanding, focusing on the use of wetlands,  
65 continental shelves and the open ocean to enhance natural CO<sub>2</sub> removal processes. One  
66 marine CDR method under investigation is ocean alkalinity enhancement (OAE), which aims  
67 to accelerate the ocean CO<sub>2</sub> uptake through weathering, namely the breakdown of rocks  
68 and minerals by water-induced chemical reactions whereby atmospheric CO<sub>2</sub> is consumed  
69 and eventually stored in the ocean for millenia.

70 OAE can be realised by releasing alkaline minerals or solutions at the ocean surface,  
71 which would chemically convert aqueous CO<sub>2</sub> (CO<sub>2</sub>(aq)) into stable bicarbonate (HCO<sub>3</sub><sup>-</sup>) and  
72 carbonate (CO<sub>3</sub><sup>2-</sup>) ions, that together constitute the dissolved inorganic carbon (DIC) pool.  
73 This process would lower the ocean CO<sub>2</sub> partial pressure (pCO<sub>2</sub>) and allow for additional  
74 CO<sub>2</sub> uptake from the atmosphere to restore the altered equilibrium. Additionally, by  
75 increasing the ocean's buffering capacity, OAE would have the benefit of temporarily  
76 reducing seawater acidification.

77 CO<sub>2</sub> seasonality is a major component of the annual net ocean flux. It is mainly  
78 controlled by sea surface temperature (SST), its thermal component, and DIC, its  
79 biophysical component (Fassbender et al., 2022). SST acts on the chemical solubility of  
80 gases in seawater, favouring CO<sub>2</sub> dissolution in winter and CO<sub>2</sub> outgassing in summer  
81 (Williams & Follows, 2011). Conversely, DIC leads to CO<sub>2</sub> loss in winter, when enhanced  
82 vertical mixing and organic matter (OM) respiration increase carbon content at the top  
83 layer, and to CO<sub>2</sub> uptake in summer, when OM production prevails and reduces surface DIC.  
84 As SST and DIC are counteracting drivers (Lerner et al., 2021; Gallego et al., 2018, Takahashi  
85 et al., 2002), the one that dominates determines the ocean's role as either a net annual  
86 CO<sub>2</sub> source or sink at a given location.

87 Changes to the CO<sub>2</sub> flux seasonality can further perturb the ocean carbon cycle,  
88 including earlier calcium carbonate undersaturation (Kwiatkowski et al., 2022) and  
89 intensified ocean acidification (Sasse et al., 2015), other than acting upon inter-annual  
90 variability patterns (Rustogi et al., 2023). Moreover, the ocean pCO<sub>2</sub> seasonal cycle is  
91 expected to increase due to rising atmospheric CO<sub>2</sub> concentrations and a higher oceanic  
92 CO<sub>2</sub> background, independently of the seasonal driver (Gallego et al., 2018).

93 Although OAE has been widely investigated to account for theoretical benefits and  
94 challenges, little attention has been given to its effects on the seasonal carbon cycle. For  
95 example, OAE could cause asymmetrical or phase shifts to the air-sea CO<sub>2</sub> flux, or alter  
96 seasonal extrema. These modifications could in turn affect the ocean's net annual uptake,



97 with potential reflections on marine ecosystems at different scales. Additionally, while the  
98 atmosphere reacts to system stimuli at short timescales, the ocean system can take  
99 several seasons to respond (Salt et al., 2013) and understanding such time lags is  
100 necessary to account for OAE impacts. Lastly, OAE efficiency would likely be influenced by  
101 changes to the Revelle factor, which quantifies the ocean's sensitivity to pH changes  
102 resulting from increasing atmospheric CO<sub>2</sub>; the lower the Revelle factor, the larger the  
103 seawater buffering capacity against CO<sub>2</sub> perturbations (Egleston et al., 2010). For example,  
104 Schwinger et al. (2024) found that, per unit of alkalinity addition, higher atmospheric CO<sub>2</sub>  
105 drives larger ocean uptake mainly because of the associated chemical efficiency.

106 To address these knowledge gaps, we explored seasonal carbon dynamics using  
107 output data from an earth system model (ESM) that simulated OAE along the European  
108 coastline under a low- and a high-emission Shared Socio-economic Pathway (SSP)  
109 (SSP1-2.6 and SSP3-7.0, respectively). Our study aims to (a) analyse the impacts of OAE on  
110 seasonal carbon cycle components, and (b) evaluate the influence of the background  
111 climate scenario on such outcomes.

112

## 113 2 Materials and Methods

### 114 2.1 Earth System Model

115 The simulations used in this manuscript were run using the Flexible Ocean and Climate  
116 Infrastructure (FOCI) ESM (Matthes et al., 2020). FOCI consists of an  
117 atmosphere–ocean–sea ice general circulation model with a surface land component,  
118 coupling the Nucleus for European Modelling of the Ocean (NEMO3.6, Madec and The  
119 NEMO Team, 2015) for ocean and sea-ice, the Jena Scheme for Biosphere–Atmosphere  
120 Coupling in Hamburg (JSBACH; Brovkin et al., 2013) for the land, and  
121 ECHAM6.3-HAM2.3-MOZ1.0 (ECHAM6-HAMMOZ; Schultz et al., 2018) for the atmosphere.  
122 The ocean is divided into 46 vertical layers with a horizontal resolution of 1/2° and the  
123 atmosphere is composed of 95 vertical layers with a horizontal resolution of ~1.8°.

124 In addition to simulating the land carbon cycle, FOCI incorporates the Model of  
125 Oceanic Pelagic Stoichiometry (MOPS) (Kriest & Oschlies, 2015) to enable the  
126 representation of marine biogeochemical processes and the ocean carbon cycle. MOPS  
127 resolves biological dynamics such as phytoplankton carbon uptake and remineralisation,  
128 calcite formation and dissolution (Chien et al., 2022).

129 In FOCI, both alkalinity and DIC agree well with observations, while still showing a  
130 positive bias at the surface and a negative bias below 3000 meters of depth (Chien et al.,  
131 2022). Most DIC variations are due to OM build-up and CO<sub>2</sub> flux variations, while alkalinity is  
132 a prognostic tracer simulated as a combination of biological sources and sinks with:



133 nitrate and phosphate supply as sinks, calcium carbonate production and dissolution as  
134 sink and source, respectively, and OM formation and remineralisation as sink and source,  
135 respectively (Chien et al., 2022).

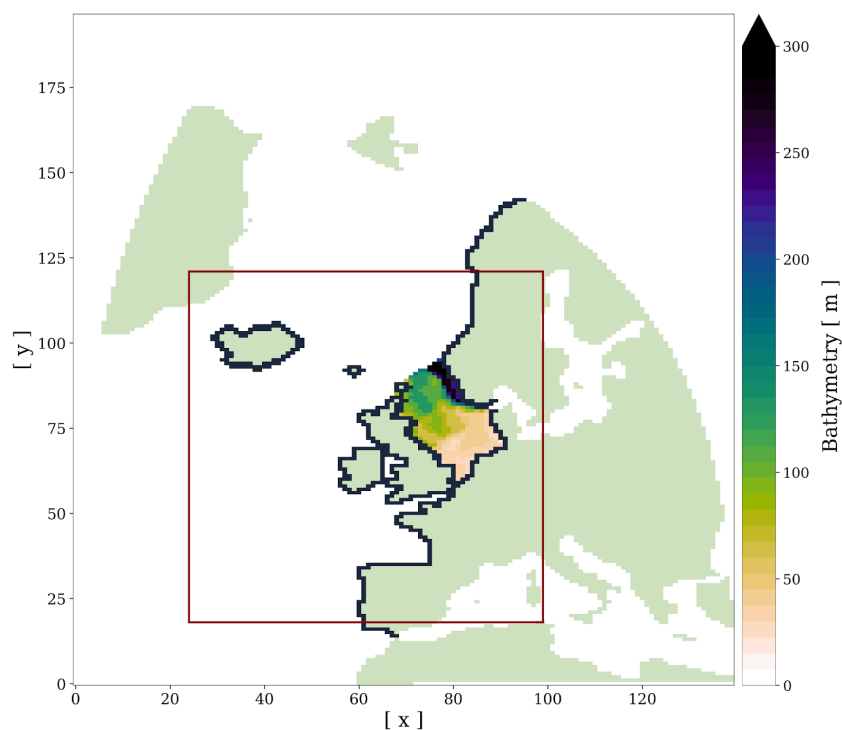
136

### 137 2.1 Experimental design

138 A 1500-year spin-up was carried out with 'physics-only' FOCL, followed by a 500-year  
139 spin-up including MOPS (Chien et al., 2022). Then, historical simulations were run from  
140 1850 to 2014, when the SSPs begin (Riahi et al., 2017). All spin-ups, baseline simulations  
141 and forcings adhered to the CMIP6 protocol (O'Neill et al., 2016). In order to investigate the  
142 role of the climate scenario on OAE application, a low- and high-emission SSP have been  
143 selected, namely SSP1-2.6 and SSP3-7.0. Simulations were run in emission-driven mode,  
144 such that atmospheric carbon is exchanged with the ocean and the terrestrial biosphere.

145

146 Figure 1: Spatial implementation of OAE in European waters. The black strip indicates a  
147 50-km-wide zone of alkalinity addition, while the red rectangle marks the study area  
148 analysed in this manuscript. The map also shows the bathymetry of the North Sea,  
149 identified as a key hotspot region in this analysis.



150

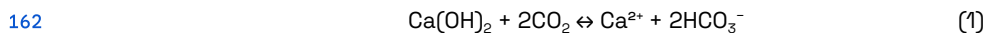


151

152 In the OAE simulations, alkalinity is added continuously and uniformly along a  
153 50-km-wide strip of the European coastline, with the exclusion of the Baltic and  
154 Mediterranean seas (fig. 1). OAE is applied from 2025 to 2100, with linear increase over the  
155 first decade of addition (2025-2034), until the alkalinity equivalent of 1 Gt  $\text{y}^{-1}$  of  
156 fast-reacting calcium hydroxide ( $\text{Ca}(\text{OH})_2$ ) is reached. From 2035, this amount, equal to 1.4  
157  $\mu\text{mol C m}^{-2} \text{y}^{-1}$ , is held constant until the end of the century.

158 Theoretically,  $\text{Ca}(\text{OH})_2$  consumes two moles of atmospheric  $\text{CO}_2$  and produces one  
159 mole of calcium ( $\text{Ca}^{2+}$ ) and two moles of bicarbonate, therefore increasing alkalinity by a  
160 factor of two (eq. (1)) (Chien et al., 2022):

161



163

### 164 2.3 Data processing

165 The global output data delivered by FOCL was sliced to the European region, depicted  
166 by the red rectangle in fig. 1. This helps maintain some focus beyond the European  
167 coastline without diluting the OAE signal, as Palmiéri & Yool (2024) showed that part of the  
168 OAE-driven carbon uptake can happen far from the implementation region. Our analysis  
169 compares the area of coastal addition (black line in fig. 1), which offers details on regime  
170 shifts taking place at the epicenter of the domain, with the European region (including its  
171 coastline), which measures how the European system as a whole might respond to OAE.

172 Assuming that the most visible baseline-to-OAE differences are detected towards the  
173 end of the century, the annual cycle averaged over the last simulation decade  
174 (2090-2099) is considered here. While ocean  $\text{pCO}_2$  and the  $\text{CO}_2$  flux are written out only for  
175 the surface, alkalinity is calculated over all 46 FOCL ocean layers. Thus, the variable was  
176 vertically averaged over a seasonally- and scenario-dependent mixed layer depth (MLD)  
177 (also a FOCL output variable defined from potential density), which is the region in direct  
178 contact with the atmosphere. The alkalinity that is subducted below the MLD is assumed  
179 not to induce  $\text{CO}_2$  uptake by the ocean on short timescales (He & Tyka, 2023).

180

## 181 3 Results

### 182 3.1 The baseline seasonal state in the study area

183 Being a continental shelf pump, the North Sea (NS) plays an important role in carbon  
184 uptake by transferring atmospheric  $\text{CO}_2$  into interior waters and ultimately to the open

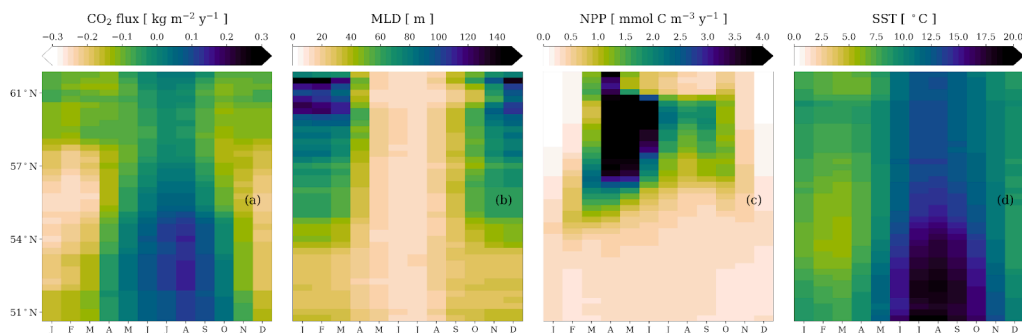


185 ocean (Prowe et al., 2009). Furthermore, this is the region where the OAE-driven seasonal  
186 change signal is strongest in our model. To provide context for interpreting the results, we  
187 thus analyse the SSP1-2.6 baseline seasonal state in the NS for the CO<sub>2</sub> flux (fig. 2a) and  
188 for its driving variables: MLD (fig. 2b), surface net primary production (NPP) (fig. 2c), and  
189 SST (fig. 2d).

190 In line with previous research, the seasonal air-sea CO<sub>2</sub> flux in the study area is  
191 characterised by two biogeochemical provinces, one in the North and the other in the  
192 South (Thomas et al., 2004). Biology dominates in the seasonally-stratified northern NS,  
193 where winter mixing deepens the mixed layer (fig. 2b) and replenishes surface nutrients.  
194 With the onset of spring stratification, the resulting shallow MLD retains nutrients in the  
195 euphotic zone, supporting high NPP (fig. 2c) and sequentially driving CO<sub>2</sub> uptake (fig 2a).  
196 Accumulated OM then sinks below the surface layer, where remineralisation can happen  
197 far from atmospheric contact. At this location, CO<sub>2</sub> sequestration through carbon fixation  
198 outweighs temperature-driven outgassing, turning the area into a strong carbon sink (Salt  
199 et al., 2013; Prowe et al., 2009).

200

201 Figure 2: Hovmöller diagram of the zonally-averaged North Sea section for the  
202 SSP1-2.6 baseline seasonal cycle of (a) the CO<sub>2</sub> flux, (b) mixed layer depth (MLD), (c)  
203 surface net primary production (NPP), and (d) sea surface temperature (SST) over the  
204 2090-2099 mean. In the CO<sub>2</sub> flux plot, negative values indicate ocean uptake.



205

206

207 In the southern NS and the adjacent European continental shelf, the air-sea CO<sub>2</sub>  
208 exchange is primarily controlled by SST (fig. 2d) (Salt et al., 2013). Due to the shallow NS  
209 bathymetry (fig. 1) and limited MLD variation (fig. 2b), a well-mixed water column is created  
210 year-round. This prevents the seasonal build-up and re-entrainment of nutrients  
211 remineralised below the surface during summer, thereby limiting new NPP (fig. 2c). The  
212 southern NS is a region of weak CO<sub>2</sub> source to the atmosphere (fig. 2a), as the OM



213 production and remineralisation happen within the same surface compartment, where CO<sub>2</sub>  
214 can easily be exchanged with the atmosphere, and community respiration outweighs  
215 photosynthetic activity (Artioli et al., 2012, Prowe et al., 2009, Thomas et al., 2004).

216

### 217 3.2 OAE-driven modifications to the seasonal carbon cycle

218 For the European average in SSP1-2.6 (fig. 3a), baseline surface alkalinity has lowest  
219 values in summer and highest values in winter, with respective extremes of 2198 and 2209  
220  $\mu\text{mol kg}^{-1}$ . With OAE, alkalinity increases throughout the year: SSP1-2.6 baseline values are  
221 higher than SSP3-7.0 (fig. 3b), although OAE increases surface alkalinity relatively less  
222 than under high emissions. Under both scenarios, the largest change happens in August.

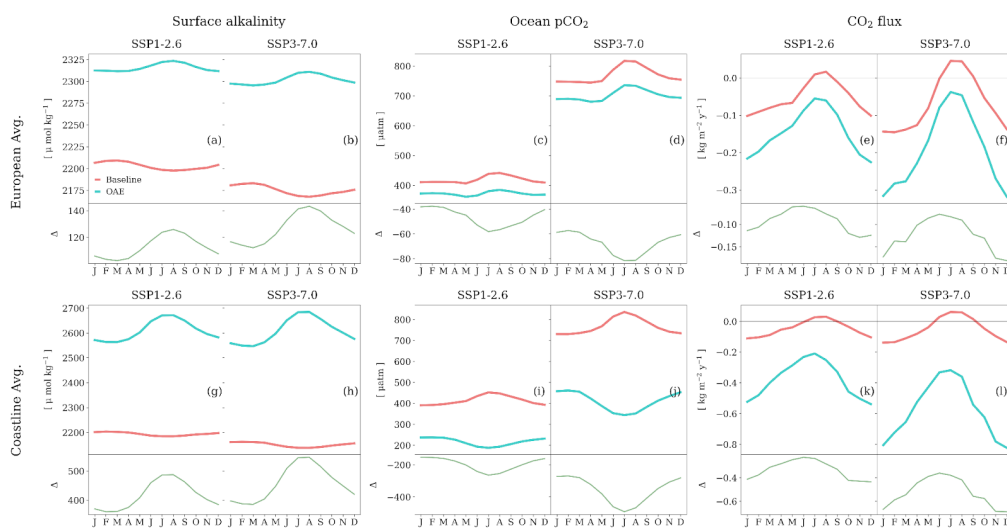
223 At the coastline (fig. 3g, h), OAE increases surface ocean alkalinity up to 2672  $\mu\text{mol}$   
224  $\text{kg}^{-1}$  in SSP1-2.6 and 2685  $\mu\text{mol kg}^{-1}$  in SSP3-7.0, both in summer. Furthermore, the  
225 amplitude of the seasonal cycle increases slightly compared to the baseline, amounting  
226 to 108  $\mu\text{mol kg}^{-1}$  and to 138  $\mu\text{mol kg}^{-1}$  in the low- and high-emission scenario, respectively.

227 Under both scenarios and in both coastal and European waters, alkalinity addition  
228 reverses its surface seasonal cycle, with summer values exceeding winter values. While  
229 under natural conditions, alkalinity increases with depth, and winter mixing helps  
230 replenish the upper ocean from deeper layers, in the OAE simulations, alkalinity is added at  
231 the surface, and stronger vertical stratification in summer leads to greater alkalinity  
232 retention in the top layer.

233

234 Figure 3: Seasonal cycle averaged over 2090-2099 for surface alkalinity, ocean pCO<sub>2</sub>, and  
235 the CO<sub>2</sub> flux, with the OAE-baseline difference depicted by the green line. From left to  
236 right, columns indicate the European average (top) in SSP1-2.6 (a, c, e) and in SSP3-7.0 (b,  
237 d, f), and the coastline average (bottom) in SSP1-2.6 (g, i, k) and in SSP3-7.0 (h, j, l). In the  
238 CO<sub>2</sub> flux plots, negative values indicate ocean uptake.

239



240

241

242 Under both SSPs, the MLD-averaged alkalinity spatial pattern reveals strongest  
243 variation in the southern NS as well as by the UK coastline, where the seasonal amplitude  
244 grows strongly. In SSP3-7.0 (fig. 4c), the seasonal amplification signal extends over a  
245 slightly wider area than in SSP1-2.6 (fig. 4a), while open ocean regions like Iceland, Spain  
246 and Norway show less strong changes compared to the baseline.

247 For ocean pCO<sub>2</sub>, the European average in SSP1-2.6 (fig. 3c) is characterised by lowest  
248 and highest values in May and August, respectively, with a mean seasonal amplitude of 35  
249 μatm. Ocean pCO<sub>2</sub> minima are identified in spring as a result of phytoplankton bloom and  
250 consequent high NPP (fig. 2c), whereby CO<sub>2</sub> is drawn down by photosynthetic fixation. In  
251 the OAE simulation, ocean pCO<sub>2</sub> absolute values drop and the amplitude decreases from 35  
252 μatm to 23 μatm in SSP1-2.6 and from 73 μatm to 55 μatm in SSP3-7.0.

253 At the coastline, ocean pCO<sub>2</sub> is directly influenced by the OAE-driven reversal of the  
254 alkalinity seasonal cycle: highest (lowest) summer (winter) values in the baseline become  
255 lowest (highest) in the OAE scenario. In SSP1-2.6 (fig. 3i), ocean pCO<sub>2</sub> decreases by about  
256 200 μatm, and the amplitude is reduced by 11 μatm. In SSP3-7.0 (fig. 3j), OAE doubles the  
257 reduction of ocean pCO<sub>2</sub> values compared to SSP1-2.6 and values become similar to the  
258 low warming baseline, though the amplitude is enhanced by 11 μatm.

259 OAE reduces surface ocean pCO<sub>2</sub> in all cases, with the strongest variation occurring in  
260 summer, when natural ocean pCO<sub>2</sub> reaches its peak. This indicates that, in our simulations,  
261 alkalinity addition produces the greatest pCO<sub>2</sub> decline during periods of natural CO<sub>2</sub>  
262 outgassing. At the European average, this results in a reduction of the seasonal pCO<sub>2</sub>  
263 amplitude that is more pronounced under low emissions. Along the coastline, while

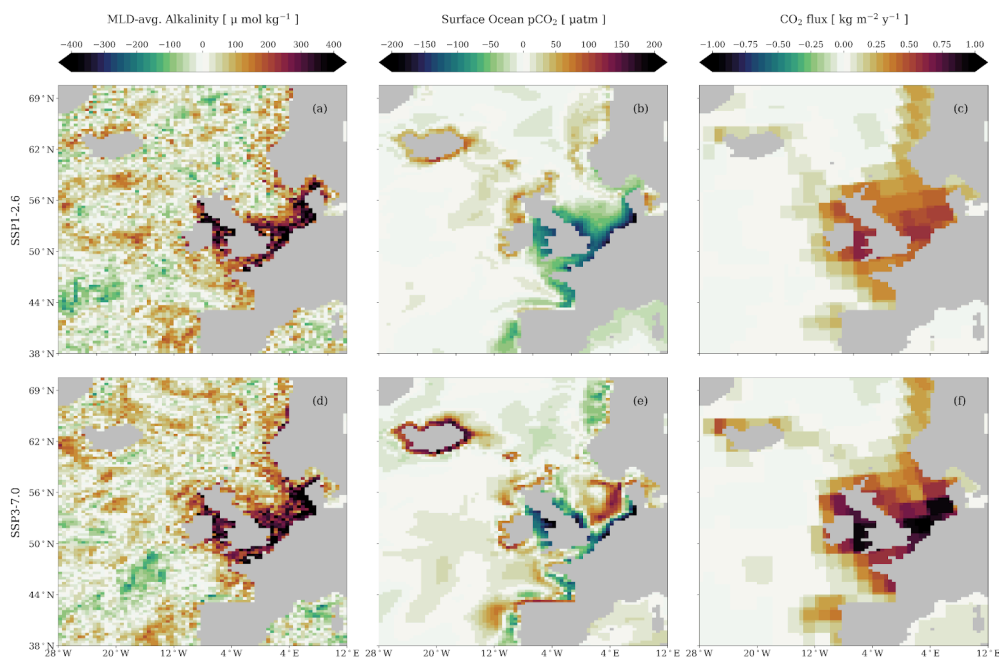


264 SSP1-2.6 shows an amplitude reduction, SSP3-7.0 leads to an amplitude increase. Thus,  
265 while in a low-warming climate, alkalised water becomes less sensitive to DIC fluctuations,  
266 higher atmospheric CO<sub>2</sub> partially counteracts the buffering effect driven by alkalinity  
267 addition, leading to a higher Revelle factor.

268

269 Figure 4: Seasonal amplitude change (OAE - baseline) averaged over 2090-2099 for (a, d)  
270 MLD-averaged alkalinity, for (b, e) ocean pCO<sub>2</sub> and for (c, f) the air-sea CO<sub>2</sub> flux. The top row  
271 is SSP1-2.6 and the bottom row is SSP3-7.0. CO<sub>2</sub> flux calculations are performed on the  
272 atmospheric component of FOCL, which has a coarser resolution than the ocean  
273 component.

274



275

276

277 In SSP1-2.6 (fig. 4b), a distinct spatial pattern of pCO<sub>2</sub> seasonal change is identified,  
278 with two diverging geographies: at higher latitudes, including Iceland, the Norwegian and  
279 British North-West bank, the seasonal amplitude is slightly more pronounced than the  
280 baseline, while at lower latitudes, namely the mainland shoreline and the  
281 central-to-southern UK coasts, the seasonal cycle is strongly mitigated. In SSP3-7.0 (fig.  
282 4e), results are magnified in Iceland, in the Southern NS, in the UK and Irish coasts.  
283 Exceptions are found in the central NS and Northern Spain, where strong seasonal



284 amplification is displayed, and by the Norwegian coast, where the ocean  $p\text{CO}_2$  seasonal  
285 cycle is reduced.

286 As for the  $\text{CO}_2$  flux, seasonality is driven by temperature in our study area: the system  
287 outgasses (takes up)  $\text{CO}_2$  in summer (winter), at lowest (highest) chemical solubility, and  
288 the largest  $\text{CO}_2$  release happens between July and August. Alkalinity addition enhances  
289 the  $\text{CO}_2$  flux seasonal cycle everywhere and under both warming scenarios, turning the  
290 system into a  $\text{CO}_2$  sink year-round.  $\text{CO}_2$  uptake grows more strongly in winter, meaning that  
291 alkalisation impacts are largest when ocean uptake is naturally highest, and in SSP3-7.0,  
292 meaning that the system becomes more sensitive under higher emissions.

293 For the European average, OAE-induced  $\text{CO}_2$  flux amplitude has an average span of  
294  $0.171 \text{ kg m}^{-2} \text{ yr}^{-1}$  in SSP1-2.6 and  $0.281 \text{ kg m}^{-2} \text{ yr}^{-1}$  in SSP3-7.0, compared to their  
295 respective baselines ( $0.118 \text{ kg m}^{-2} \text{ yr}^{-1}$  and  $0.191 \text{ kg m}^{-2} \text{ yr}^{-1}$ ). At the coastline in the  
296 OAE-driven SSP1-2.6 simulation, the  $\text{CO}_2$  flux seasonal amplitude is  $0.329 \text{ kg m}^{-2} \text{ yr}^{-1}$ ,  
297 therefore more than doubling the baseline amplitude of  $0.114 \text{ kg m}^{-2} \text{ yr}^{-1}$ . With an  
298 amplitude of  $0.505 \text{ kg m}^{-2} \text{ yr}^{-1}$ , the OAE seasonal  $\text{CO}_2$  flux in SSP3-7.0 is more than 2.5  
299 times larger than the baseline ( $0.199 \text{ kg m}^{-2} \text{ yr}^{-1}$ ). Spatially, in SSP1-2.6, the OAE scenario  
300 reveals largest  $\text{CO}_2$  seasonal flux amplification along the European continental coastline,  
301 and the signal remains strong until the connection with the open ocean (fig. 4c). Seasonal  
302 amplification is enhanced under high emissions (fig. 4f), especially in the southern NS, at  
303 the UK coastline and in North-West Iceland.

304

## 305 5 Discussion

306 Our results show that significant system perturbations happen within the model  
307 domain, especially in close proximity to the alkalinity addition site. However, this  
308 manuscript does not address alkalised water that is subducted before air-sea equilibration  
309 is complete, and uncertainty remains on whether that water could resurface to drive  $\text{CO}_2$   
310 uptake elsewhere. In Palmiéri & Yool (2024), for example, it was estimated that about 50%  
311 of  $\text{CO}_2$  uptake favoured by global coastal OAE happened remotely from the alkalinity  
312 injection sites.

313 In agreement with Schwinger (2022), OAE works to amplify the  $\text{CO}_2$  seasonal flux,  
314 prompting greater carbon uptake during winter. This is because OAE effects are larger in  
315 the season where higher  $\text{CO}_2$  drawdown occurs naturally. Additionally, OAE-induced  
316 modifications to ocean  $p\text{CO}_2$  are highest in the season where the associated seasonal  
317 driver reduces the ocean  $\text{CO}_2$  sink potential, as alkalised water minimises  $p\text{CO}_2$  sensitivity  
318 to DIC flux modulations and strengthens the ocean's buffering capacity, thus lowering the  
319 Revelle factor. Spatial variations across latitudes may result from contrasting responses



320 between semi-enclosed regions and the open ocean, or from differences in the local  
321 seasonal driver of the carbon cycle.

322 Both in European waters and at the coastline, highest alkalinity is recorded between  
323 the end of summer and the onset of autumn, but the largest CO<sub>2</sub> uptake occurs in winter,  
324 thus introducing a response lag of a few weeks. Jones et al. (2014) note that air-sea  
325 equilibration can take from a few months to even years to complete, depending on  
326 regional properties. Considering the physical features of the southern NS, where a shallow  
327 water column is well-mixed throughout the year, OAE is likely to encourage fast  
328 equilibration and allow for efficient carbon sequestration under enhanced alkalinity.

329 In the OAE simulations, the seasonal cycle of surface alkalinity is reversed under both  
330 SSPs, especially in summer. However, its absolute levels increase relatively more in  
331 SSP3-7.0 compared to SSP1-2.6 because vertical stratification, and therefore surface  
332 retention, is larger in a high CO<sub>2</sub> world. Ocean pCO<sub>2</sub> absolute values show a less significant  
333 decline in SSP1-2.6 compared to SSP3-7.0, although the amplitude compression signal is  
334 stronger in the former. Exceptionally, the SSP3-7.0 coastline amplitude is enhanced, as its  
335 sensitivity due to rising temperatures outweighs reduced sensitivity due to alkalinity  
336 addition. For the CO<sub>2</sub> flux, since the seasonal amplification is stronger in SSP3-7.0, higher  
337 background emissions makes the system more susceptible to external alterations. As  
338 noted by Nagwekar et al. (2024), this is probably more linked to the ocean carbonate  
339 chemistry, which becomes more sensitive under high CO<sub>2</sub> emissions, than to the  
340 background atmospheric CO<sub>2</sub> concentration (Schwinger et al., 2024).

341 Our results indicate that OAE-induced impacts on the seasonal cycle of ocean pCO<sub>2</sub>  
342 and the CO<sub>2</sub> flux are spatially- and scenario-dependent. Spatially, the most affected area  
343 is the North Sea, especially its southern part, and the coastal ocean between the UK and  
344 Ireland, which show pronounced seasonal alterations. A shallow, well-mixed and  
345 partially-enclosed sea allows for alkalinity to accumulate at the surface, rather than being  
346 lost due to subduction to deeper layers or advection to the open ocean (Liu et al., 2025;  
347 Wang et al., 2023). As for the influence of the climate scenario, the seasonal sensitivity of  
348 the ocean carbon cycle increases with larger CO<sub>2</sub> emissions and OAE alone is less efficient  
349 in mitigating seasonal amplitude changes in the high-emissions scenario compared to the  
350 low-emission scenario. Furthermore, higher atmospheric CO<sub>2</sub> concentrations, which have  
351 an amplifying effect on the thermally-driven component of ocean pCO<sub>2</sub>, lead to an overall  
352 expansion of the CO<sub>2</sub> seasonal cycle due to stronger chemical leverage. This outcome is  
353 exacerbated by OAE implementation due to the scenario-dependent chemical efficiency  
354 of OAE (Schwinger et al., 2024).

355

356 6 Conclusions



357 This study addressed the OAE-driven variations to the seasonal carbon cycle in  
358 European waters under low and high warming, contributing to the understanding of CO<sub>2</sub>  
359 intra-annual variability when continuous coastal OAE is applied. It was found that, in a  
360 region of temperature-driven seasonality, (a) OAE enhances the CO<sub>2</sub> uptake in winter, when  
361 it is naturally strongest, and it reduces ocean pCO<sub>2</sub> in summer, when it is naturally highest;  
362 (b) the sensitivity of the seasonal carbon cycle increases under higher emissions,  
363 enhancing the CO<sub>2</sub> flux seasonal amplification and contrasting the pCO<sub>2</sub> seasonal  
364 dampening; (c) locations like the southern North Sea could be ideal to implement OAE, as a  
365 shallow bathymetry and intense mixing can hasten the CO<sub>2</sub> gas transfer at the air-sea  
366 interface, at least as far as the equilibration timescale is shorter than the surface water  
367 mean residence time.

368 Some limitations and future recommendations can be drawn from this study. Firstly,  
369 while freshwater input from rivers is modelled in FOCl, riverine alkalinity is not accounted  
370 for, limiting the reliability of absolute values. Alkalinity in the Baltic Sea, for example, is  
371 poorly resolved by FOCl, which could have an impact on the NS boundary conditions.  
372 Additionally, as river runoff features are deeply seasonal, implementing such processes  
373 would improve the accuracy of future simulations. Secondly, our analysis does not  
374 separate the CO<sub>2</sub> flux into its thermal and biological element, therefore missing to discern  
375 the influence that each has in altering the CO<sub>2</sub> seasonal cycle. Given the significance of  
376 temperature variability in the southern NS, calculating both terms individually could  
377 provide further insight into their seasonal role under OAE deployment. Lastly, our OAE  
378 simulations picture a highly idealised scenario, which is unlikely to become a real-world  
379 case. Other, more realistic OAE techniques should be explored, such as pulsed or  
380 point-source experiments. Building on these simulations, further investigation is therefore  
381 recommended to set the premises for a conscious large-scale OAE application.

382

### 383 7 Author contribution

384 Conceptualisation: C. Ciscato, D. P. Keller; Performing model simulations: T. P. Kemena;  
385 Data curation: C. Ciscato, D. P. Keller; Formal analysis: C. Ciscato; Investigation: C. Ciscato;  
386 Methodology: D. P. Keller, T. P. Kemena; Supervision: D. P. Keller; Validation: D. P. Keller;  
387 Visualisation: C. Ciscato; Writing – original draft: C. Ciscato; Writing – review & editing: C.  
388 Ciscato, D. P. Keller, N. Mehendale, T. P. Kemena, S. Avrutin.

389

### 390 8 Acknowledgements and financial support

391 C.C. acknowledges funding from German BMBF, Project RETAKE, and from the European  
392 Union's Horizon Europe research and innovation programme under grant agreements no.



393 101056939 (RESCUE). This is a contribution to the CDRmare research mission funded by  
394 the German Alliance for Marine Research (DAM). D.P.K. acknowledges funding from the  
395 European Union's Horizon 2020 research and innovation programme under grant  
396 agreement no. 869357 (project OceanNETs). The authors acknowledge the use of Python  
397 for analysis and graphics in this paper. The authors acknowledge the computing time  
398 made available on the high-performance computer "Lise" at the NHR center NHR@ZIB  
399 (former HLRN). This center is jointly supported by the Federal Ministry of Education and  
400 Research and the state governments participating in the NHR.

401

#### 402 9 Data availability

403 The datasets used in this manuscript are available at this Zenodo link  
404 ([https://zenodo.org/records/13935197?token=eyJhbGciOiJIUzUxMiJ9.eyJpZCI6Ijg2ZWViNjU0LWMyZDYtNGFmZC04MzI0LWUxMmE5YTlhMzdhNyIsImRhdGEiOiNt9LCJyYW5kb20iOiIyODIyODFjZmUwZTk2MzJjOTcxNGM2ZWZmZWwzMWwzNDYwMjY5LnN5S8fH7EYBkEYYP9xUI\\_P2V4L4HUKBYEi61fFGDd43WwMskAWQBsnCFdpBMYii\\_TpWstwKQbsFSCF2K\\_\\_F4oQ](https://zenodo.org/records/13935197?token=eyJhbGciOiJIUzUxMiJ9.eyJpZCI6Ijg2ZWViNjU0LWMyZDYtNGFmZC04MzI0LWUxMmE5YTlhMzdhNyIsImRhdGEiOiNt9LCJyYW5kb20iOiIyODIyODFjZmUwZTk2MzJjOTcxNGM2ZWZmZWwzMWwzNDYwMjY5LnN5S8fH7EYBkEYYP9xUI_P2V4L4HUKBYEi61fFGDd43WwMskAWQBsnCFdpBMYii_TpWstwKQbsFSCF2K__F4oQ)).

408 The code underlying this study is openly available at the following GitHub repository:  
409 2026 ciscato oae seasonality  
410 ([https://github.com/chiaraciscato/2025\\_ciscato\\_oae\\_seasonality](https://github.com/chiaraciscato/2025_ciscato_oae_seasonality)).

411

#### 412 10 References

413 Artioli, Y., Blackford, J. C., Butenschön, M., Holt, J. T., Wakelin, S. L., Thomas, H., and Allen, J. I.: The  
414 carbonate system in the North Sea: Sensitivity and model validation, *Journal of Marine Systems*,  
415 **102**, 1–13, 2012.

416 Brovkin, V., Boysen, L., Raddatz, T., Gayler, V., Loew, A., and Claussen, M.: Evaluation of vegetation  
417 cover and land-surface albedo in MPI-ESM CMIP5 simulations, *Journal of Advances in Modeling  
418 Earth Systems*, **5**, 48–57, 2013.

419 Chien, C.-T., Durgadoo, J. V., Ehlert, D., Frenger, I., Keller, D. P., Koeve, W., et al.: FOCI-MOPS v1 –  
420 Integration of marine biogeochemistry within the Flexible Ocean and Climate Infrastructure  
421 version 1 (FOCI) Earth system model, *Geoscientific Model Development Discussions*, 1–58, 2022.

422 Fassbender, A. J., Schlunegger, S., Rodgers, K. B., and Dunne, J. P.: Quantifying the role of  
423 seasonality in the marine carbon cycle feedback: An ESM2M case study, *Global Biogeochemical  
424 Cycles*, **36**, e2021GB007018, 2022.



- 425 Friedlingstein, P., O'Sullivan, M., Jones, M. W., Andrew, R. M., Gregor, L., Hauck, J., et al.: Global  
426 carbon budget 2022, *Earth System Science Data*, **14**, 4811–4900, 2022.
- 427 Gallego, M. A., Timmermann, A., Friedrich, T., and Zeebe, R. E.: Drivers of future seasonal cycle  
428 changes in oceanic pCO<sub>2</sub>, *Biogeosciences*, **15**, 5315–5327, 2018.
- 429 He, J. and Tyka, M. D.: Limits and CO<sub>2</sub> equilibration of near-coast alkalinity enhancement,  
430 *Biogeosciences*, **20**, 27–43, 2023.
- 431 Jones, D. C., Ito, T., Takano, Y., and Hsu, W.-C.: Spatial and seasonal variability of the air–sea  
432 equilibration timescale of carbon dioxide, *Global Biogeochemical Cycles*, **28**, 1163–1178, 2014.
- 433 Kriest, I. and Oeschler, A.: MOPS-1.0: Towards a model for the regulation of the global oceanic  
434 nitrogen budget by marine biogeochemical processes, *Geoscientific Model Development*, **8**,  
435 2929–2957, 2015.
- 436 Kwiatkowski, L., Torres, O., Aumont, O., and Orr, J. C.: Modified future diurnal variability of the  
437 global surface ocean CO<sub>2</sub> system, *Global Change Biology*, 2022.
- 438 Lerner, P., Romanou, A., Kelley, M., Romanski, J., Ruedy, R., and Russell, G.: Drivers of air–sea CO<sub>2</sub>  
439 flux seasonality and its long-term changes in the NASA-GISS model CMIP6 submission, *Journal of*  
440 *Advances in Modeling Earth Systems*, **13**, e2019MS002028, 2021.
- 441 Liu, F., Daewel, U., Kossack, J., Demir, K. T., Thomas, H., and Schrum, C.: Evaluating ocean alkalinity  
442 enhancement as a carbon dioxide removal strategy in the North Sea, *EGUsphere*, 1–34, 2025.
- 443 Madec, G. and the NEMO Team: NEMO ocean engine (Version 3.6 stable), Note du Pôle de  
444 modélisation de l'Institut Pierre-Simon Laplace, No. 27, ISSN 1288-1619, 2015.
- 445 Matthes, K., Biastoch, A., Wahl, S., Harlaß, J., Martin, T., Brücher, T., et al.: The Flexible Ocean and  
446 Climate Infrastructure version 1 (FOCI): Mean state and variability, *Geoscientific Model*  
447 *Development*, **13**, 2533–2568, 2020.
- 448 Nagwekar, T., Nissen, C., and Hauck, J.: Ocean alkalinity enhancement in deep water formation  
449 regions under low and high emission pathways, *Earth's Future*, **12**, e2023EF004213, 2024.
- 450 O'Neill, B. C., Tebaldi, C., van Vuuren, D. P., Eyring, V., Friedlingstein, P., Hurtt, G., et al.: The Scenario  
451 Model Intercomparison Project (ScenarioMIP) for CMIP6, *Geoscientific Model Development*, **9**,  
452 3461–3482, 2016.
- 453 Palmiéri, J. and Yool, A.: Global-scale evaluation of coastal ocean alkalinity enhancement in a  
454 fully coupled Earth system model, *Earth's Future*, **12**, e2023EF004018, 2024.



455 Prowe, A. F., Thomas, H., Pätsch, J., Kühn, W., Bozec, Y., Schiettecatte, L.-S., and de Baar, H. J.:  
456 Mechanisms controlling the air–sea CO<sub>2</sub> flux in the North Sea, *Continental Shelf Research*, **29**,  
457 1801–1808, 2009.

458 Riahi, K., van Vuuren, D. P., Kriegler, E., Edmonds, J., O’Neill, B. C., Fujimori, S., et al.: The Shared  
459 Socioeconomic Pathways and their energy, land use, and greenhouse gas emissions  
460 implications: An overview, *Global Environmental Change*, **42**, 153–168, 2017.

461 Rustogi, P., Landschützer, P., Brune, S., and Baehr, J.: The impact of seasonality on the annual  
462 air–sea carbon flux and its interannual variability, *npj Climate and Atmospheric Science*, **6**, 66,  
463 2023.

464 Egleston, E. S., Sabine, C. L., and Morel, F. M.: Revelle revisited: Buffer factors that quantify the  
465 response of ocean chemistry to changes in DIC and alkalinity, *Global Biogeochemical Cycles*, **24**,  
466 2010.

467 Salt, L. A., Thomas, H., Prowe, A. F., Borges, A. V., Bozec, Y., and de Baar, H. J.: Variability of North  
468 Sea pH and CO<sub>2</sub> in response to North Atlantic Oscillation forcing, *Journal of Geophysical*  
469 *Research: Biogeosciences*, **118**, 1584–1592, 2013.

470 Sasse, T., McNeil, B., Matear, R., and Lenton, A.: Quantifying the influence of CO<sub>2</sub> seasonality on  
471 future aragonite undersaturation onset, *Biogeosciences*, **12**, 6017–6031, 2015.

472 Schultz, M. G., Stadtler, S., Schröder, S., Taraborrelli, D., Franco, B., Krefting, J., et al.: The  
473 chemistry–climate model ECHAM6.3-HAM2.3-MOZ1.0, *Geoscientific Model Development*, **11**,  
474 1695–1723, 2018.

475 Schwinger, J.: Report on modifications of ocean carbon cycle feedbacks under ocean  
476 alkalization, 2022.

477 Schwinger, J., Bourgeois, T., and Rickels, W.: On the emission–path dependency of the efficiency  
478 of ocean alkalinity enhancement, *Environmental Research Letters*, **19**, 074067, 2024.

479 Scott-Buechler, C. M. and Greene, C. H.: Role of the ocean in climate stabilization, in: *Bioenergy*  
480 *with Carbon Capture and Storage*, 109–130, 2019.

481 Takahashi, T., Sutherland, S. C., Sweeney, C., Poisson, A., Metzl, N., Tilbrook, B., et al.: Global sea–air  
482 CO<sub>2</sub> flux based on climatological surface ocean pCO<sub>2</sub> and seasonal biological and temperature  
483 effects, *Deep Sea Research Part II: Topical Studies in Oceanography*, **49**, 1601–1622, 2002.

484 Thomas, H., Bozec, Y., Elkalay, K., and de Baar, H. J.: Enhanced open ocean storage of CO<sub>2</sub> from  
485 shelf sea pumping, *Science*, **304**, 1005–1008, 2004.



- 486 Wang, H., Pilcher, D. J., Kearney, K. A., Cross, J. N., Shugart, O. M., Eisaman, M. D., and Carter, B. R.:  
487 Simulated impact of ocean alkalinity enhancement on atmospheric CO<sub>2</sub> removal in the Bering  
488 Sea, *Earth's Future*, **11**, e2022EF002816, 2023.
- 489 Williams, R. G. and Follows, M. J.: *Ocean Dynamics and the Carbon Cycle: Principles and*  
490 *Mechanisms*, Cambridge University Press, 2011.